METHODS AND RESOURCES

RUNNING HEAD: Precise oxygen control in brain slice recordings

Precise Dynamic Control of Tissue Oxygenation during Brain Slice Electrophysiology

Alicia Jurado[1,2,†], Anna P. Pérez-González[3,4,†], Ramon Farré[1,2,4], David Gozal[5], Xavier Gasull[3,4] and Isaac Almendros[1,2,4,*]

[1] Unitat de Biofísica i Bioenginyeria, Facultat de Medicina i Ciències de la Salut, Universitat de Barcelona, Barcelona, Spain
[2] CIBER de Enfermedades Respiratorias, Madrid, Spain
[3] Laboratori de Neurofisiologia, Departament de Biomedicina, Facultat de Medicina, Institut de Neurociències, Universitat de Barcelona, Barcelona, Spain
[4] Institut d'Investigacions Biomèdiques August Pi i Sunyer, Barcelona, Spain
[5] Office of The Dean and Department of Pediatrics, Joan C. Edwards School of Medicine, Marshall University, WV, USA
[†] These authors contributed equally to this work.

Correspondence: *Isaac Almendros. Unitat de Biofísica i Bioenginyeria. Facultat de Medicina i Ciències de la Salut, Universitat de Barcelona. Casanova 143, 08036 Barcelona, Spain. Email: isaac.almendros@ub.edu. Tel: +34 934 02 4515*

UPDATED February 2025

ABSTRACT

Precise oxygen regulation is essential for maintaining neuronal integrity in ex vivo brain slice electrophysiology, yet conventional chambers provide poorly defined oxygenation. This limitation is particularly problematic when model neurological disorders characterized by transient or intermittent hypoxia (IH), such as transient ischemic attacks and sleep apnea. We aimed to develop a versatile Oxyslice Recording Chamber (ORC) enabling real-time monitoring of neural activity with rapid, precise oxygen modulation during standard recordings. A polydimethylsiloxane (PDMS)-based ORC comprising a gas-permeable membrane that separates the recording and gas chambers was developed, allowing rapid and uniform oxygen exchange. The device integrates seamlessly into standard electrophysiological setups and operates at low perfusion rates. Tissue oxygenation was measured, and hippocampal slices were exposed to continuous hypoxia (CH, 3% or 1% O_2) and IH (6-1% O_2 cycles every 30 s), while recording field excitatory postsynaptic potentials (fEPSPs) in the hippocampal CA1 region. The ORC achieved precise, reproducible control of oxygen at the cellular level. Both CH and IH induced hypoxia severity–dependent reductions in fEPSP slopes, fully reversed upon reoxygenation. Severe CH (1% O_2) reduced the fEPSP slope by ~60%, whereas IH reduced it by ~40%, indicating a partial mitigation during reoxygenation phases. This novel ORC provides a robust, adaptable method for real-time oxygen modulation in ex vivo neuronal standard recordings. Its ability to model continuous and intermittent hypoxia at physiological oxygen tensions fills a major gap in current electrophysiological methodologies, opening new opportunities for mechanistic studies of hypoxia-driven dysfunction and therapeutic discovery.

NEW & NOTEWORTHY

This study presents the Oxyslice Recording Chamber (ORC), a simple and reproducible system for precise oxygen control during brain slice recordings. The ORC has been developed to be easily constructed and implemented in any electrophysiology laboratory. As proof of concept, we reproduced continuous hypoxia (transient ischemic stroke) and intermittent hypoxia (sleep apnea), revealing distinct and reversible changes in hippocampal function applicable to various hypoxia-related conditions and brain regions.

Keywords: Electrophysiology; oxygen control, precise-cut brain slices; transient ischemic stroke; obstructive sleep apnea.

UPDATED February 2025

INTRODUCTION

Brain slice electrophysiology is a widely used approach to investigate neuronal function under controlled ex vivo conditions (1). It enables researchers to isolate specific brain regions and neural circuits, providing valuable insights into synaptic transmission, cell excitability, and pharmacological responses in different neuronal disease models (1–3). Living neuronal cells in freshly cut tissue slices still requires continuous oxygen supply to generate energy through cellular respiration, which is essential for nerve impulse transmission (4,5). Conversely, insufficient tissue oxygen deliver can impair cell viability and alter electrophysiological properties. Most studies use pre-oxygenated artificial cerebrospinal fluid (aCSF) to preserve neurological activity in submerged chambers (5,6). The oxygen levels applied to the tissue slices are generally monitored only in the perfusion system instead of being directly measured at the tissue/cellular level (7–10). Consequently, the actual O_2 concentration reaching the cells within the tissue slice remains uncontrolled, thereby explaining the standard use of hyperoxic aCSF (95% O_2 saturated) (7–10). In addition, Ivanov et al. uncovered that neuronal activity and oxidative metabolism in mouse hippocampal slices also require a high perfusion rate (~15 ml/min with 95% O_2) to ensure sufficient oxygenation to maintain stable local field potentials and sustain predictable spontaneous/pharmacologically induced network activity and short-term synaptic plasticity (5). Interestingly, when a 95% O_2 solution is applied to tissue samples exposed to ambient air during electrophysiological measurements, two common problems frequently occur: 1) the oxygen concentration in the sample tends to stabilize by ambient air diffusion through the media (11); 2) the neuronal cells are exposed to hyperoxia considering that the actual physiological O2 values measured in vivo, i.e. physioxia, are ~6% O_2 (12,13). This is of relevance since neurons are likely altered under hyperoxic conditions during which reactive oxygen species (ROS) will be generated and lead to neuronal damage and mitochondrial dysfunction (14). In addition, the actual amount of oxygen that reaches a specific region also depends on the gas diffusion through the tissue and the depth from the surface where the electrophysiological recording is made (15). Thus, the accurate regulation and monitoring of oxygen levels in brain slices is crucial, not only for conventional electrophysiologic assessments, but particularly when examining conditions characterized by disease-specific patterns of intermittent or continuous hypoxia, as experienced by patients suffering from either obstructive or central sleep apnea or from transient ischemic attacks (TIA). Indeed, electrophysiological recordings of animals exposed to hypoxia have shown alterations in hippocampal excitatory and inhibitory neurons and network activity (16). These alterations could be associated with regional brain abnormalities after TIA events (17), as well as be manifested by cognitive and behavioral dysfunction as reported in sleep apnea patients (18–20).

The frequent inconsistent results during standard electrophysiological procedures using brain slices may in fact be due to the lack of precise oxygenation control. To overcome these limitations, some investigators have proposed small microfluidic devices capable of controlled oxygen delivery (21–25). In general, these approaches aim to reduce the aCSF volume to obtain a more homogeneous and stable value of O_2 at a tissular level. However, these experimental systems are difficult to reproduce in other laboratories, as they require the assembly of different complex components, the use of sophisticated techniques such soft lithography (22), and in most cases, oxygen is still supplied by perfusion of a pre-oxygenated culture medium (21,23–26).

UPDATED February 2025

MATERIALS AND METHODS

Design and development of an ORC for controlled gas delivery in ex vivo brain electrophysiological recordings

As illustrated in Figure 1A and 1B, the novel ORC is composed of two compartments: an upper recording chamber and a lower gas chamber, separated by a thin gas-permeable polydimethylsiloxane (PDMS) membrane (165 µm thick; Gel-Pak, Hayward, CA, USA). PDMS exhibits high oxygen permeability, optical transparency, and biocompatibility, properties that facilitate its use in physiological recordings chambers (27). This membrane allows for fast diffusion of gases between both chambers (time constant ≈1-2 s (28)). The recording chamber is fabricated using a 3D-printed negative mold designed with Ultimaker Cura software (Ultimaker, Utrecht, Netherlands) (file available in supplementary materials) and printed in polycarbonate using an Ultimaker S5 printer. A 10:1 mixture of PDMS prepolymer and curing agent (Sylgard 184 kit, Dow Corning, MI) was poured into the mold and cured at 65ºC for 1 h (Selecta, Barcelona, Spain). The recording chamber, which was designed by replicating a standard slice recording chamber, was bonded to the PDMS membrane by activating both surfaces with a corona treater (Electro Technic Products, Chicago, IL) for 1 min. To obtain the gas chamber, a 9.2 cm^2 Petri dish was drilled at its edge creating two opposite holes and attached to the rest of the ORC with non-polymerized PDMS at 65ºC for 2 h (video available in supplementary materials). All gas mixtures (with different O_2 concentrations and always balanced in 5% CO_2 and N_2) were generated using a servo-controlled gas blender (McQ, 141 Virginia, USA) controlled by the Gas Mixture Creator software (McQ, Virginia, USA). The gas mixture at room temperature was applied at flow rate of 180 mL/min into the gas chamber via a tube connected to one of the Petri dish's inlet ports. The gas was released through the opposite outlet port, ensuring a continuous air stream at atmospheric pressure across the chamber. Consequently, air circulating in the gas chamber diffused through the membrane to reach the brain slice placed on top of it.

Real-time oxygen concentration within brain slices was measured using a fiber-optic oxygen microsensor (OXR50, PyroScience, Aachen, Germany; 50 µm tip diameter, response time <2 s for 90% signal shift). Before measurements, the oxygen probe was calibrated according to the manufacturer's instructions, using two reference solutions: air-saturated water (20% O_2) and an oxygen-free solution (0.1M $C_6H_7NaO_6$ and NaOH). Then, the sensor was attached to a vertical positioning holder with micrometric resolution, and the oxygen concentration was measured at a depth of 30 µm from the slice surface, corresponding to the depth at which electrophysiological recordings are routinely performed. Temperature was constantly controlled with a temperature probe (TSUB36; PyroScience, Aachen, Germany) placed in the artificial cerebrospinal fluid 2 (aCSF2) solution within the recording chamber. The slice was stabilized using a platinum U-shaped slice anchor with nylon yarns, ensuring mechanical support throughout the experiments. Considering that O_2 must diffuse through the sample, the correlation between the O_2 applied in the gas chamber and the actual value of O_2 at tissue level was assessed (Figure 1C).

Preparation of precision-cut brain slices

C57BL/6N mice (2-4 months old) were anesthetized using isoflurane and decapitated. Brains were rapidly removed and immersed for 2 minutes in ice-cold artificial cerebrospinal fluid 1 (aCSF1) containing the following (in mM): 206 Sucrose, 11 Glucose, 1.25 NaH_2PO_4, 26 $NaHCO_3$, 1.3 KCl, 1 $CaCl_2$, and 10 $MgSO_4$. The solution was continuously bubbled with carbogen (95% O_2, 5% CO_2) and adjusted to pH 7.35. After removing olfactory bulbs and cerebellum, coronal slices (380 µm thickness) were

prepared using a vibrating microtome (VT1200 S; Leica Microsystems, Wetzlar, Germany) in the same cold solution. Slices were immediately incubated in a recovery chamber filled with aCSF2 at 34ºC for 1 h. The composition of aCSF2 consisted of (in mM): 11 Glucose, 1.25 NaH_2PO_4, 25 $NaHCO_3$, 2.5 KCl, 2.5 $CaCl_2$, 1.5 $MgSO_4$, and 119 NaCl, continuously bubbled with carbogen and pH adjusted to 7.35. aCSF1 (high sucrose-based) protects tissue during slicing by reducing excitotoxicity at low temperature, while aCSF2 (physiological NaCl-based) enables slice recovery and normal neuronal activity recording. Slices were subsequently incubated at room temperature for at least 1 h before starting the experimentation. All animal procedures were approved and conducted in accordance with the Ethical Committee for Animal Research from the University of Barcelona (CEEA-UB) (protocols 455/25 and 456/25) in compliance with the European and Spanish regulations.

Electrophysiology

Brain slices were transferred into the customized recording chamber which was continuously perfused (1 mL/min) with non-oxygenated aCSF2 solution at 27ºC for field excitatory post-synaptic potential (fEPSP) recordings (Figure 1D). Prior to each experiment, the PDMS membrane of the recording chamber was treated in a plasma cleaner (PDC-002, Harrick Scientific Products Inc. Pleasantville, NY) for 2 min to ensure uniform distribution of the aCSF2 solution. Thereafter, a bipolar stimulation electrode was placed in the Schaffer collateral pathway, while a recording electrode filled with aCSF2 was positioned in the dendritic branching of the CA1 area of the hippocampus. Stimulation currents ranging from 5 to 130 µA were delivered using an A385 stimulus isolation unit (WPI, Hertfordshire, UK). Before fEPSPs recordings, Input-Output (IO) curves were recorded for each slice at 0.03 Hz. The stimulation current was then adjusted for each recording to evoke fEPSPs at which the slope was at 50–60 % of maximally evoked fEPSP slope value. Paired-pulse fEPSPs were measured at 0.03 Hz with an interstimulus interval of 50 and 100 ms. All recordings were amplified and stored using an AxoClamp 2B amplifier (Molecular Devices, San Jose, CA). Tracings were analyzed using Axon pClamp software (Molecular Devices, version 10.6).

Assessment of synaptic activity at different levels of oxygen

To evaluate the impact of different oxygen levels on synaptic activity, hippocampal slices were exposed to a stepwise decrease in oxygen concentration while continuously recording field excitatory postsynaptic potentials (fEPSPs). The slices were first exposed to 22% O_2, and the oxygen level was then reduced by 2% every 5 minutes until reaching 2% O_2, followed by a final step at 1% O_2. Electrophysiology recordings were performed at 30 µm depth from the tissue surface, at the same level as the oxygenation measurements were done previously. This protocol was carried out using the oxygen-controlled recording ORC described above, enabling real-time monitoring of synaptic responses under defined oxygen conditions.

Synaptic activity changes observed in experimental models of transient ischemic stroke and sleep apnea

Brain slices were first maintained under physiological brain oxygen concentration (6% O_2) (12,13) for 15 min to establish a stable synaptic response prior to hypoxic exposures. To replicate a transient ischemic attack, brain slices were maintained to continuous mild (3% O_2) or severe hypoxia (1% O_2) for 30 min. In another set of experiments, we reproduced the intermittent hypoxia (IH) that occurs in OSA patients. Specifically, the brain slices were subjected to cycles of 6% / 1% O_2 for 30 s each, for a total of 30 min. At the end of the hypoxic exposures, slices were returned to 6% O_2 for a recovery period.

UPDATED February 2025

Statistical analysis

All results are shown as mean ± standard error of the mean (SEM), except where otherwise noted in the text. To compare the fEPSP slope values obtained in the same brain region at different oxygen concentrations, a one-way repeated-measures analysis of variance (ANOVA) was performed, followed by Dunnett's post hoc test for comparisons with the control (brain physioxia, 6% O_2). To compare the different variables between groups in the TIA and OSA models, a two-way repeated-measures ANOVA (variables: tissue oxygenation and time) was performed, followed by the Student Newman Keuls post hoc test. All analyses were done using statistical software (SigmaPlot 11.0; Systat Software, Inc., San Jose, CA). A $p \leq 0.05$ was considered statistically significant.

RESULTS

We developed a PDMS-based ORC enabling precise control of oxygen delivery to brain slices while simultaneously allowing neuronal recordings. The desired oxygen levels were supplied by a gas blender into the gas chamber and diffused through the PDMS membrane into the tissue. Oxygen concentration was measured at 30 µm below the tissue surface using an oxygen microsensor (Figure 1B). A clear linear correlation was observed between the oxygen concentration delivered by the gas blender and that measured within the brain slice, allowing for accurate calibration of the system (Figure 1C). We designed this model inspired by a standard electrophysiological recording plate to enable easy adaptation and implementation by other laboratories.

Effect of different oxygen levels on synaptic activity

This novel ORC enables real-time assessment of oxygen-dependent neuronal activity, as demonstrated by fEPSP recordings in the CA1 region of mouse hippocampal slices (Figure 2). To investigate how different oxygenation levels influence synaptic transmission, fEPSPs were measured in brain slices exposed to progressively decreasing O_2 concentrations, ranging from 22% to 1% (severe hypoxia) (Figure 2). Interestingly, the response profile exhibited a clear asymmetry around physioxia (6% O_2), a typical oxygenation level observed in brain tissue in vivo (12,13). On the hyperoxic side, a slight fEPSP slope potentiation was observed only at higher oxygen levels (~19% increase at 22% O_2 compared to baseline at 6% O_2). In contrast, the fEPSP slope dropped sharply on the hypoxic side, with significant reductions at 2% O_2 (74.82 ± 4.91%, $p<0.001$) and 1% O_2 (65.36 ± 4.44%, $p<0.001$) compared to baseline (100 ± 3.93%). No changes in fEPSP values were observed under continuous 6% oxygen during 1h (Supplementary Figure).

Reversible impairment of synaptic activity under mild and severe transient hypoxic-ischemic conditions

To assess the effects of a prolonged period of hypoxia followed by reoxygenation on synaptic transmission as occurs in a transient ischemic stroke, hippocampal slices were exposed to either mild (3% O_2) or severe (1% O_2) hypoxia for 30 min, followed by a recovery period. As shown in Figure 3A and 3B, the ORC reduced the oxygen availability in brain tissue oxygenation from baseline (6% O_2) to the final hypoxic values within approximately 30 s. When hypoxia was induced in brain tissue, the fEPSP slope progressively decreased during the first 5-10 min before reaching a stable level (Figure 3A and 3B). As expected, the exposure to severe hypoxia elicited a more pronounced and sustained reduction of the fEPSP slope (41.89 ± 7.34%, $p<0.001$) vs. baseline, compared to mild hypoxia (76.82 ± 7.15%, $p<0.05$) (Figure 3C). Interestingly, during mild hypoxia, the fEPSP slope remained relatively stable throughout the

hypoxic period showing a minimal reduction of ~3%, whereas in severe hypoxia the slope declined more markedly (~10% reduction), suggesting cumulative neuronal fatigue and a trend to reduce synaptic resilience under prolonged severe oxygen deprivation in contrast to mild hypoxia ($p=0.074$). Upon reoxygenation, both conditions showed substantial recovery, reaching ~95–100% of baseline values. The quantitative analysis also revealed that at least 15 min are needed to achieve a nearly complete recovery. In addition, short-term synaptic plasticity was evaluated by paired-pulse stimulation at 50 and 100 ms interstimulus intervals before and after hypoxic challenge (Figure 3D). However, no significant changes were observed in the paired-pulse ratio (PPR) after both hypoxic conditions.

Intermittent hypoxia mimicking sleep apnea induces reversible synaptic dysfunction

As shown in Figure 4A, the novel ORC successfully generated IH exposures in brain slices, oscillating from ~6% to 1% and mimicking the changes observed in severe obstructive sleep apnea patients. During IH exposures, fEPSP significantly decreased compared to baseline levels ($63.38 \pm 12.30\%$, $p<0.05$), indicating impaired synaptic transmission under IH conditions (Figure 4B and 4C). After IH recovery, fEPSP slope increased significantly (103.62 ± 12.39, $p<0.05$), reaching baseline values within 15 min (101.66 ± 1.40, ns). Therefore, the synaptic function is reversible after 30 min of IH exposures.

Finally, PPR analysis at interstimulus intervals of 50 ms and 100 ms revealed no significant differences between pre- and post-IH conditions (Figure 4D), suggesting that short-term presynaptic plasticity was not significantly affected by IH exposures.

UPDATED February 2025

DISCUSSION

In this study, we developed and validated a simple and easy to reproduce PDMS-based ORC that enables fast and precise control of oxygen levels in brain slices, while simultaneously allowing for standard electrophysiological recordings. This system offers a physiologically relevant platform to study how oxygen fluctuations, ranging from hyperoxia to severe hypoxia may affect synaptic function. This novel ORC reproduces multiple oxygen-related neuropathological scenarios, including continuous and intermittent hypoxia, thereby enabling the replication of several diseases such as TIA and sleep apnea. As a proof of concept aimed at establishing the relevance of controlling oxygenation in brain slices, we show that within a few minutes, both sustained hypoxia and IH induce marked but reversible synaptic impairments. Thus, the current study provides a novel in vitro model that permits the dissection of the neural consequences of the transient oxygen instability that occurs in very prevalent disorders such as OSA and central sleep apnea.

The experimental ORC is based on a gas-permeable PDMS membrane to separate the gas and recording chambers. Notably, gas equilibration across the PDMS membrane occurs in less than 2 seconds (15,29), allowing for rapid oxygen exchange. As a result, the final oxygen concentration at the tissue level where electrophysiological recordings are performed is reached within approximately 30 s following a change in gas composition which is controlled by the gas blender (Figures 3A, 3B and 4A). In this context, our experimental system overcomes the limitation of reduced oxygen delivery to the tissue typically observed in conventional submerged chambers used for neuronal recordings (5). In fact, this characteristic also allows the application of high-frequency IH in brain slices, a feature that is of particular interest for studies focused on brain responses to oxygenation changes mimicking sleep apnea (15). Nevertheless, due to the high cellular density and oxygen consumption in brain tissues (25,26), oxygen availability is probably not completely homogeneous across the full thickness of the slice, decreasing with the distance from the oxygen source (11,15,25). Accordingly, in the present study, we have taken into consideration the brain slice thickness typically used in electrophysiological recordings, as well as the insertion depth of the electrodes used for stimulation and signal acquisition. By establishing a linear and predictable relationship between the delivered gas composition and the oxygen concentration detected within the tissue at the stimulation sites, we ensured precise control and accurate calibration of the oxygenation environment during neuronal recordings (Figure 1C).

In recent years, several microfluidic-based models have been developed to enhance oxygen and nutrient supply in brain slices. These systems have been conceptualized for specific applications, such as minimizing bubbling artifacts, enabling localized oxygen delivery (22), and creating low-volume incubation chambers to perform multisite recording (23,24), to enrich the cellular secretome, and to reduce drug consumption (21). However, their fabrication often requires complex microfluidic techniques (23,24) along with onerous lithography procedures (22) , making them technically challenging to implement and replicate in other neurophysiology laboratories. Consequently, these models have not been routinely adopted in a quest to achieve precise regulation and monitoring of oxygen levels during neuronal recordings. In contrast, the ORC developed herein was specifically designed for easy integration into any neurophysiology laboratory setup. To this end, the recording chamber was designed based on the geometry of a standard electrophysiological chamber, providing full compatibility with conventional recording systems. Furthermore, considering the oxygen diffusion properties of the PDMS membrane, gas exchange occurs homogeneously across the whole tissue sample. Also, the rapid oxygen diffusion facilitates a substantial reduction in the perfusion rate required

to maintain tissue oxygenation. Specifically, a relatively low perfusion rate of 1 mL/min, when coupled with chamber-mediated oxygenation, is sufficient to sustain basal neuronal activity. Importantly, this configuration also provides flexibility to modulate oxygen levels as required, thereby offering a controlled framework for investigating oxygen-dependent neuronal processes. This perfusion rate is similar to the one used in most conventional electrophysiological recordings in brain slices, where a perfusion between 1-2 mL/min aCSF with saturated 95% O_2 / 5% CO_2 is used. Nevertheless, others have suggested that a perfusion of ~15 mL/min would be required to preserve neuronal function (5). This feature is particularly relevant given the potential damage caused by a high flow rate. In fact, the effect of shear stress on the brain has been extensively studied in the context of the blood brain barrier, showing that endothelial (30) and immune cells, among other neuronal cells, respond to this mechanical stimulus inducing their differentiation and activation, respectively (31).

In a first batch of experiments, synaptic activity was assessed in response to a range of oxygen levels (from 22% to 1% O_2; Figure 2). Our findings revealed the importance of delivering an oxygen concentration that precisely corresponds to the metabolic requirements of a specific tissue. In the brain, the physiological oxygen concentration in vivo is ~ 6% O_2 (12,13), which reflects the natural tissue oxygenation and differs significantly from the atmospheric oxygen level (~21% O_2) typically used in conventional electrophysiology experiments. Interestingly, the resulting relationship between oxygenation and fEPSPs displayed a markedly different behavior under hypoxic (<6%) and hyperoxic (>6%) conditions. Indeed, neuronal cells were significantly more sensitive to hypoxia, exhibiting a pronounced fEPSPs reduction (~35%) under the most severe condition applied (1% O_2). In contrast, increasing oxygen levels induced a less pronounced hyperactivity (up to ~20% increase at 22% O_2 when compared to physioxia). These findings also emphasize the importance of controlling oxygen levels during conventional electrophysiological recordings. The routine use of 95% O_2 can induce neuronal hyperactivity and may in fact introduce greater variability across studies (final tissue O_2 depends on oxygen diffusion and depth). Moreover, such hyperoxic levels can trigger the production and release of reactive oxygen species (ROS), which can exert neurotoxic effects (14).

As proof of concept, we also recorded neuronal activity in response to transient continuous hypoxia challenges and IH patterns that replicate those observed in TIA and sleep apnea patients, respectively. These experiments demonstrate the ORC´s capability to precisely modulate oxygen delivery at the cellular level, one of the key features of our novel platform. In this study, we simulated moderate (3% O_2) and severe (1% O_2) TIA (Figure 3). In both cases, the reduction in the field excitatory postsynaptic potential (fEPSP) slope correlated with the severity of hypoxia. Following 30 min of continuous hypoxia, synaptic function was restored upon reoxygenation with physiological oxygen levels (6% O_2). These findings are consistent with previous studies employing anoxic aCSF (95% N_2) for 10 min (10), 30 min (8), and 40 min (9), all of which reported a complete suppression of neuronal activity followed by recovery upon reoxygenation with aCSF saturated with 95% O_2. In the context of TIA, our model offers a significant advantage by enabling precise control of hypoxic exposures while operating at significantly reduced perfusion flow rates, thereby minimizing shear stress on neuronal cells. In addition, the ORC represents a significant technological advancement for sleep research. Currently, there is a lack of experimental models capable of delivering high-frequency IH while simultaneously performing electrophysiological recordings, which explains the absence of studies investigating synaptic responses to IH in brain tissue slices. In fact, all research to date has relied on brain samples obtained from animals previously exposed to IH protocols in vivo (18–20). Although these studies have reported impaired neuronal function following chronic IH exposures, it is important to note that removal of the brain tissue

and subsequent recordings under standard oxygenated conditions may allow for partial recovery of synaptic activity to occur. This possibility is supported by our findings, as shown in Figure 4. Here, we provide the first direct evidence of synaptic activity under precisely controlled IH conditions mimicking OSA. Interestingly, these findings indicate that reoxygenation periods during IH do not prevent, but do mitigate, the reduction in the fEPSP slope, limiting it to approximately 40% from baseline, compared to the ~60% decrease observed under continuous 1% O_2 hypoxia from the TIA model.

In conclusion, the versatile PDMS-based ORC presented herein is a technical breakthrough and a readily feasible set-up tool for precisely controlling and monitoring oxygen dynamics in brain slices while performing simultaneous electrophysiological recordings. Its capacity to simulate a wide range of hypoxic severities and durations should enable extensive and detailed characterization of synaptic responses and their reversibility under physiologically and pathologically relevant conditions. This platform is uniquely suited for investigation of how transient and intermittent oxygen fluctuations impact neuronal function across different animal models, including varying ages and neuropathological states. By bridging critical gaps in current experimental approaches, our model holds significant clinical relevance, offering novel opportunities to dissect the cellular and synaptic mechanisms underlying disorders linked to different patterns and severities of hypoxia such as stroke, TIA, and OSA, and ultimately, opening new possibilities for the development of targeted therapeutic strategies. Pragmatically, the setting described here does not require complex instrumentation for its construction and hence can be straightforwardly implemented in other laboratories.

DATA AVAILABILITY

A file for the 3D construction of the mold for building the ORC is included, along with a video showing its assembly. The data supporting the proof-of-concept findings have been included as part of the supplemental material.

SUPPLEMENTAL MATERIAL

Supplemental Figure S1: DOI. https://doi.org/10.6084/m9.figshare.30858125
Supplemental Video: DOI. https://doi.org/10.6084/m9.figshare.30858290
Supplemental 3D File: DOI. https://doi.org/10.6084/m9.figshare.30858308
Supplemental Raw data: DOI. https://doi.org/10.6084/m9.figshare.30858326

ACKNOWLEDGMENTS

The authors thank Miguel Ángel Rodríguez for his technical assistance

GRANTS

MICIU/AEI/10.13039/501100011033 and by FEDER, UE, PID2022-140774OB-I00 (to I.A.) and PID2023-148439OB-I00 (to R.F.)

SEPAR, 1396/2023 (to I.A.)

Generalitat de Catalunya, 2021SGR00292 (to X.G.) and 2021SGR00523 (to I.A. and R.F.).

Instituto de Salud Carlos III, Maria de Maeztu CEX2021-001159-M (to Institut de Neurociencies, Universitat de Barcelona).

UPDATED February 2025

DISCLOSURES

There are no conflicts to declare.

AUTHOR CONTRIBUTIONS

Conceived and designed research, I.A.; Performed experiments, A.J. and A.P.P-G; Analyzed data, A.J., A.P.P-G, X.G. and I.A.; Interpreted results of experiments, I.A., A.J., A.P.P-G, D.G., X.G. and R.F.; Prepared figures, A.J., I.A. and A.P.P-G; Drafted manuscript, A.J. and I.A.; Edited and revised manuscript, I.A., A.J., A.P.P-G, D.G., X.G. and R.F.; Funding acquisition, I.A. and X.G. All authors have read and agreed to the published version of the manuscript.

REFERENCES

1. **Chen H, Shi X, Guo F.** Whole-cell patch clamp and extracellular electrophysiology recordings in mouse brain slices. *STAR Protoc* 6:104008, 2025. https://doi.org/10.1016/j.xpro.2025.104008.

2. **Loryan I, Fridén M, Hammarlund-Udenaes M.** The brain slice method for studying drug distribution in the CNS. *Fluids Barriers CNS* 10(1):6, 2013. https://doi.org/10.1186/2045-8118-10-6.

3. **Accardi MV, Pugsley MK, Forster R, et al.** The emerging role of in vitro electrophysiological methods in CNS safety pharmacology. *J Pharmacol Toxicol Methods* 81:47–59, 2016. https://doi.org/10.1016/J.VASCN.2016.03.008

4. **Hájos N, Mody I.** Establishing a physiological environment for visualized in vitro brain slice recordings by increasing oxygen supply and modifying aCSF content. *J Neurosci Methods* 183(2):107-13, 2009. https://doi.org/10.1016/j.jneumeth.2009.06.005.

5. **Ivanov A, Zilberter Y.** Critical State of Energy Metabolism in Brain Slices: The Principal Role of Oxygen Delivery and Energy Substrates in Shaping Neuronal Activity. *Front Neuroenergetics* 3:9, 2011. https://doi.org/10.3389/fnene.2011.00009.

6. **Whitebirch AC.** Acute mouse brain slicing to investigate spontaneous hippocampal network activity. *J Vis Exp.* (162), 2020. https://doi.org/10.3791/61704.

7. **Díaz JCR, Jenkins PM, Pritchett DL, Jones KS.** A Novel Approach to Study Coherent γ-Band Oscillations in Hippocampal Brain Sections. *eNeuro* 10:ENEURO.0167-23.2023, 2023. https://doi.org/10.1523/ENEURO.0167-23.2023.

8. **Álvarez-Merz I, Fomitcheva IV, Sword J, et al.** Novel mechanism of hypoxic neuronal injury mediated by non-excitatory amino acids and astroglial swelling. *Glia* 70(11):2108-2130, 2022. https://doi.org/10.1002/glia.24241.

9. **Álvarez-Merz I, Luengo JG, Muñoz MD, et al.** Hypoxia-induced depression of synaptic transmission becomes irreversible by intracellular accumulation of non-excitatory amino acids. *Neuropharmacology* 190:108557, 2021. https://doi.org/10.1016/j.neuropharm.2021.108557.

10. **Zhang D, Xiong W, Chu S, et al.** Inhibition of hippocampal synaptic activity by ATP, hypoxia or oxygen-glucose deprivation does not require CD73. *PLoS One* 7(6):e39772, 2012.

UPDATED February 2025

https://doi.org/10.1371/journal.pone.0039772.
11. **Huchzermeyer C, Albus K, Gabriel HJ, et al.** Gamma oscillations and spontaneous network activity in the hippocampus are highly sensitive to decreases in pO2 and concomitant changes in mitochondrial redox state. *Journal of Neuroscience* 28(5):1153-62, 2008.
https://doi.org/10.1523/JNEUROSCI.4105-07.2008.
12. **Almendros I, Farré R, Planas AM, et al.** Tissue oxygenation in brain, muscle, and fat in a rat model of sleep apnea: Differential effect of obstructive apneas and intermittent hypoxia. *Sleep* 34(8):1127-33, 2011.
https://doi.org/10.5665/SLEEP.1176.
13. **Almendros I, Montserrat JM, Torres M, et al.** Changes in oxygen partial pressure of brain tissue in an animal model of obstructive apnea. *Respir Res* 11(1):3, 2010.
https://doi.org/10.1186/1465-9921-11-3.
14. **Simon Machado R, Mathias K, Joaquim L, et al.** Hyperoxia and brain: the link between necessity and injury from a molecular perspective. *Neurotox Res* 42(2):25, 2024.
https://doi.org/10.1007/s12640-024-00702-6.
15. **Jurado A, Ulldemolins A, Lluís H, et al.** Fast cycling of intermittent hypoxia in a physiomimetic 3D environment: A novel tool for the study of the parenchymal effects of sleep apnea. *Front Pharmacol* 13:1081345, 2023.
https://doi.org/10.3389/fphar.2022.1081345.
16. **Hencz A, Magony A, Thomas C, et al.** Mild hypoxia-induced structural and functional changes of the hippocampal network. *Front Cell Neurosci* 17:1277375, 2023.
https://doi.org/10.3389/fncel.2023.1277375
17. **Lv Y, Li L, Song Y, et al.** The local brain abnormalities in patients with transient ischemic attack: A resting-state fMRI study. *Front Neurosci* 13:24, 2019.
https://doi.org/10.3389/fnins.2019.00024.
18. **Payne RS, Goldbart A, Gozal D, Schurr A.** Effect of intermittent hypoxia on long-term potentiation in rat hippocampal slices. *Brain Res* 1029(2):195-9, 2004.
https://doi.org/10.1016/j.brainres.2004.09.045.
19. **Khuu MA, Pagan CM, Nallamothu T, et al.** Intermittent hypoxia disrupts adult neurogenesis and synaptic plasticity in the dentate gyrus. *J Neurosci.* 39(7):1320-1331, 2019.
https://doi.org/10.1523/JNEUROSCI.1359-18.2018.
20. **Tjong YW, Li MF, Hung MW, Fung ML.** Melatonin ameliorates hippocampal nitric oxide production and large conductance calcium-activated potassium channel activity in chronic intermittent hypoxia. *J Pineal Res* 44(3):234-43, 2008.
https://doi.org/10.1111/j.1600-079X.2007.00515.x.
21. **Dondzillo A, Quinn KD, Cruickshank-Quinn CI, et al.** A recording chamber for small volume slice electrophysiology. *J Neurophysiol* 114(3):2053-64, 2015.
https://doi.org/10.1152/jn.00289.2014.
22. **Mauleon G, Fall CP, Eddington DT.** Precise Spatial and Temporal Control of Oxygen within In Vitro Brain Slices via Microfluidic Gas Channels. *PLoS One* 7(8):e43309, 2012.
https://doi.org/10.1371/journal.pone.0043309.

UPDATED February 2025

23. **Blake AJ, Rodgers FC, Bassuener A, et al.** A microfluidic brain slice perfusion chamber for multisite recording using penetrating electrodes. *J Neurosci Methods* 189(1):5-13, 2010. https://doi.org/10.1016/j.jneumeth.2010.02.017.

24. **Killian NJ, Vernekar VN, Potter SM, Vukasinovic J.** A device for long-term perfusion, imaging, and electrical interfacing of brain tissue in vitro. *Front Neurosci* 10:135, 2016. https://doi.org/10.3389/fnins.2016.00135.

25. **Rivera KR, Yokus MA, Erb PD, et al.** Measuring and regulating oxygen levels in microphysiological systems: Design, material, and sensor considerations. *Analyst* 144(10):3190-3215, 2019. https://doi.org/10.1039/c8an02201a.

26. **Thompson JK, Peterson MR, Freeman RD.** Single-neuron activity and tissue oxygenation in the cerebral cortex. *Science* 299:1070-2, 2003. https://doi.org/10.1126/science.1079220.

27. **Kasahara K, Leygeber M, Seiffarth J, Ruzaeva K, Drepper T, Nöh K, et al.** Enabling oxygen-controlled microfluidic cultures for spatiotemporal microbial single-cell analysis. *Front Microbiol* 14:1198170, 2023. https://doi.org/10.3389/fmicb.2023.1198170.

28. **Farré R, Almendros I, Montserrat JM, et al.** Gas Partial Pressure in Cultured Cells: Patho-Physiological Importance and Methodological Approaches. *Front Physiol* 9:1803, 2018. https://doi.org/10.3389/fphys.2018.01803.

29. **Campillo N, Jorba I, Schaedel L, et al.** A novel chip for cyclic stretch and intermittent hypoxia cell exposures mimicking obstructive sleep apnea. *Front Physiol* 7:319, 2016. https://doi.org/10.3389/fphys.2016.00319.

30. **DeOre BJ, Partyka PP, Fan F, Galie PA.** CD44 mediates shear stress mechanotransduction in an in vitro blood-brain barrier model through small GTPases RhoA and Rac1. *FASEB Journal* 36(5):e22278, 2022. https://doi.org/10.1096/fj.202100822RR.

31. **Cibelli A, Ballesteros-Gomez D, McCutcheon S, et al.** Astrocytes sense glymphatic-level shear stress through the interaction of sphingosine-1-phosphate with Piezo1. *iScience* 27(6):110069, 2024. https://doi.org/10.1016/j.isci.2024.110069.

FIGURE LEGENDS

Figure 1. Design and validation of the Oxyslice Recording Chamber (ORC). (A) The ORC was developed by assembling a recording (upper) and a gas (lower) chamber separated by a gas-permeable PDMS membrane. **(B)** Schematic view of the ORC. A blender-generated gas mixture was directed through the gas chamber from inlet to outlet, diffusing across the PDMS membrane to the brain slice positioned above in the recording chamber. **(C)** Correlation between oxygen concentration within tissue slice (measured at 30 µm depth from the slice surface) and oxygen levels applied by the gas blender (n = 8). **(D)** Schematic representation of the recording site at the dendritic branching of the CA1 area of the hippocampus. Neuronal activity was assessed by recording the fEPSP response in the Schaffer collateral pathway of the CA1 region in mouse hippocampal slices.

UPDATED February 2025

Figure 2. Oxygen-dependent modulation of synaptic activity. (A) Time course of fEPSP slope changes during a progressive stepwise decrease in oxygen concentration. Slices were exposed to sequential reductions in O_2, starting at 22% O_2 and decreasing by 2% every 5 min until reaching 2% O_2, with a final step at 1% O_2 (n = 5). Data are color-coded according to O_2 concentration: values above 6% O_2 in blue, values below 6% O_2 in red, and 6% (brain physioxia, set at 100%) in white. **(B)** Boxplots of fEPSP slope values at different oxygen levels. Boxes represent the interquartile range (IQR, first to third quartile), the line indicates the median, and whiskers extend to 1.5 x IQR. One-way repeated-measures ANOVA followed by Dunnett's post hoc test for comparisons with physioxia (6% O_2). **p<0.01, ***p<0.001.

Figure 3. Synaptic activity under transient hypoxic ischemia. Time course of the fEPSP slope (purple circles) under hypoxia (blue line). Slices were initially maintained at 6% O_2 for 15 min, followed by 30 min of either mild (3% O_2) **(A)** or severe hypoxia (1% O_2) **(B)**, and then returned to 6% O_2 for 20 min. Representative fEPSPs traces before, during and after hypoxia are shown at the top of each graph (calibration: 1 mV, 5 ms). **(C)** Bar charts summarizing the data from panel A and B. Baseline, hypoxia and recovery values correspond to the last 5 min of each period. fEPSP slope values are normalized to baseline (3% O_2, n = 8; 1% O_2, n = 9). **(D)** Paired-pulse ratio (PPR) was assessed at two intervals (50 and 100 ms) before and after hypoxia (3% and 1% O_2). PPR was defined as the ratio (S_2/S_1) between the slope of the fEPSP elicited by the second (S_2) and the first (S_1) stimuli. No significant changes were observed before and after mild or severe hypoxia (n = 4). Two-way repeated-measures ANOVA followed by the Student-Newman-Keuls post hoc test. *p<0.05 and ***p<0.001. All data is expressed as mean ± SEM.

Figure 4. Synaptic activity under intermittent hypoxia. (A) The ORC reproduced the high-frequency intermittent hypoxia (IH) suffered by OSA patients (6% O_2 for 30 s and 1% O_2 for 30 s). Blue line shows real-time O_2 measurements. **(B)** Time course of the fEPSP slope (red circles) under IH (blue line). Slices were initially maintained at 6% O_2 for 15 min, followed by 30 min of IH, and then returned to 6% O_2 for 20 min. Representative fEPSPs traces before, during and after IH are shown at the top (calibration: 1 mV, 5 ms). **(C)** Bar charts summarizing the data from panel B. Baseline, IH and recovery values correspond to the last 5 min of each period. fEPSP slope values are normalized to baseline (n = 4). **(D)** Paired-pulse ratio (PPR) was evaluated at two intervals (50 and 100 ms) before and after IH. No significant changes were observed before and after IH (n=3). Two-way repeated-measures ANOVA followed by the Student-Newman-Keuls post hoc test. *p<0.05. All data is expressed as mean ± SEM.

UPDATED February 2025

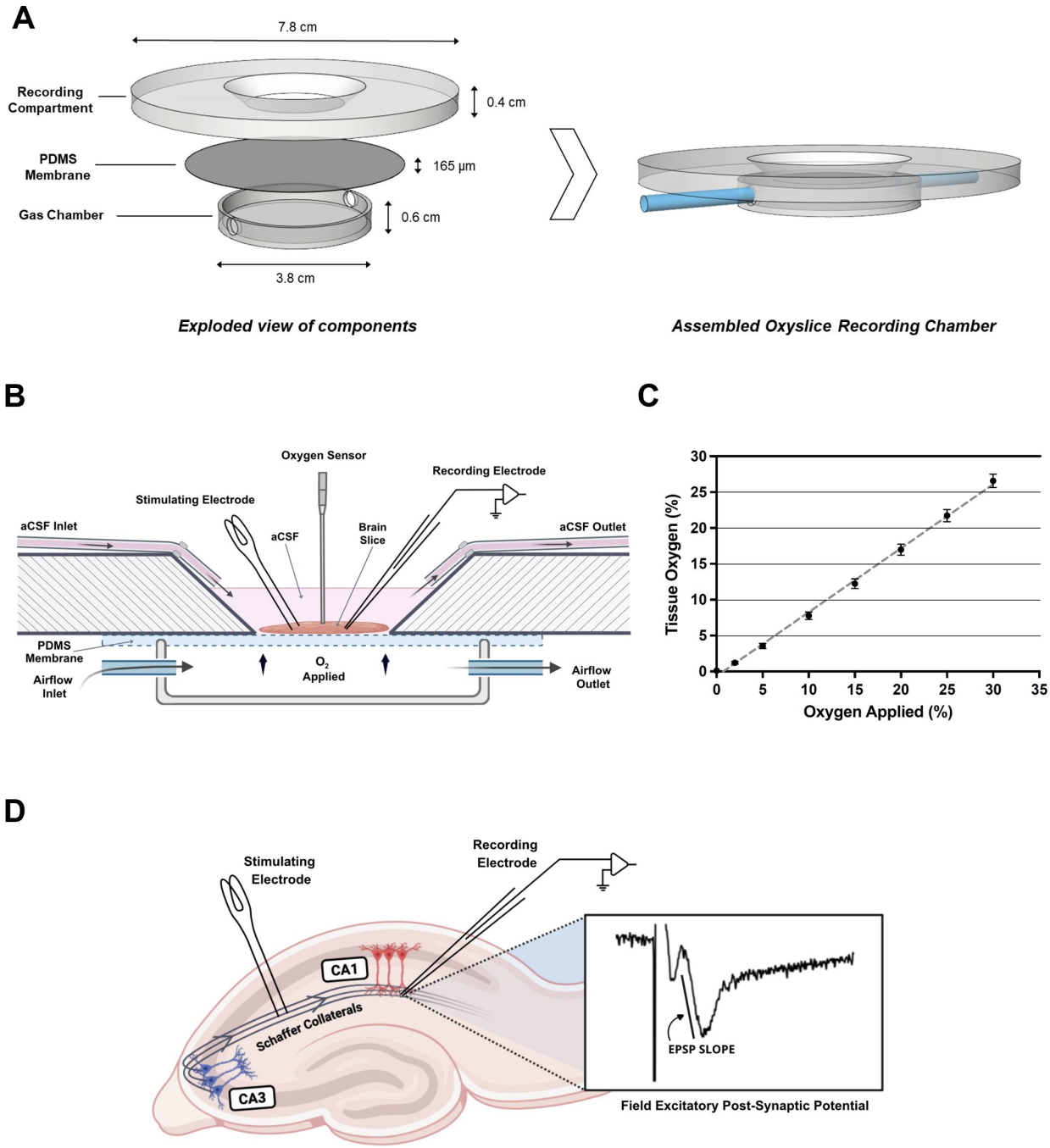

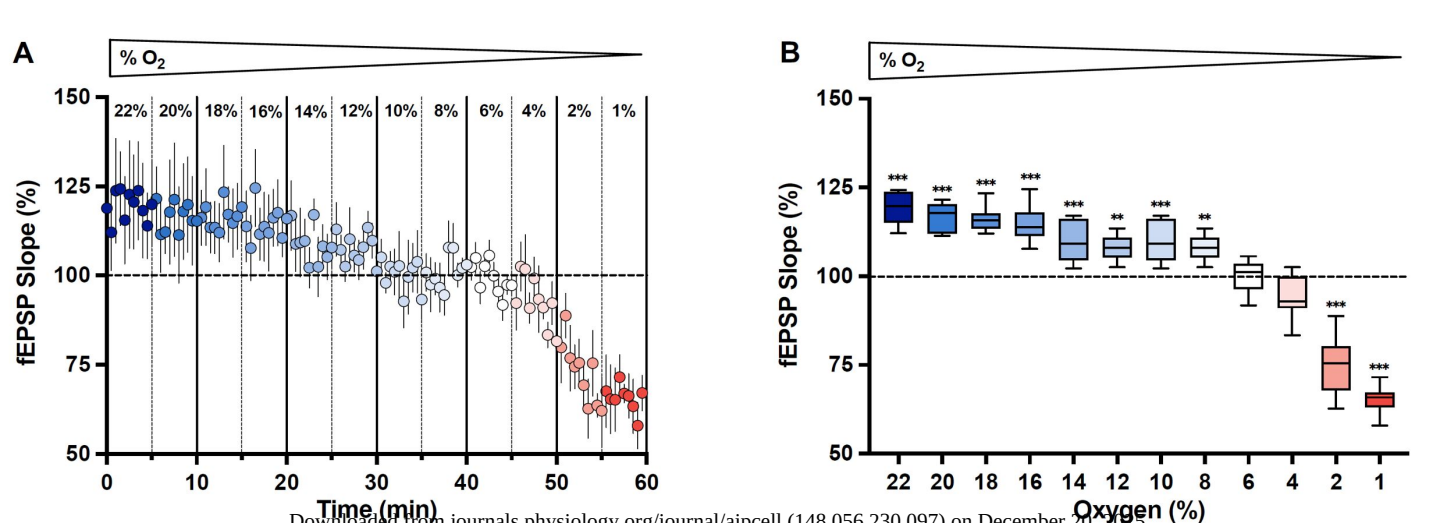

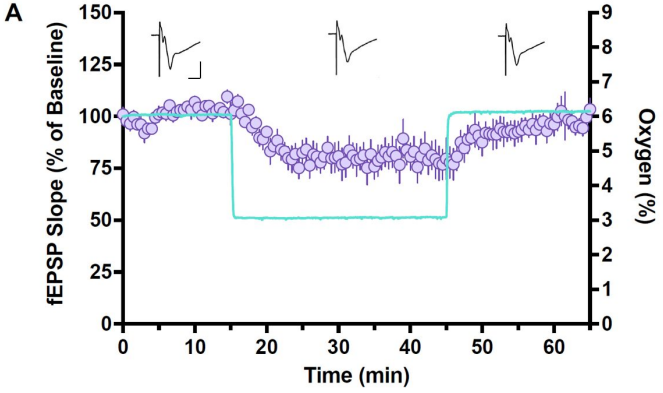

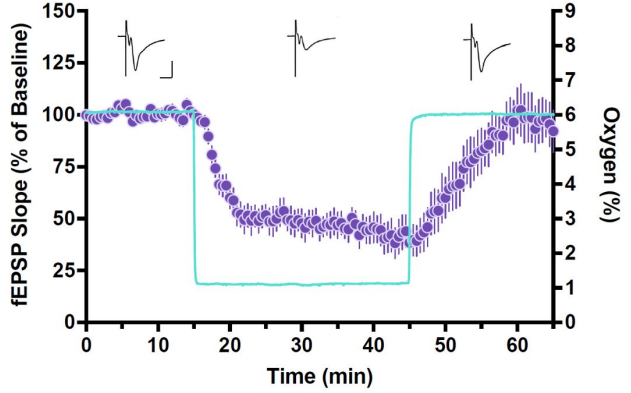

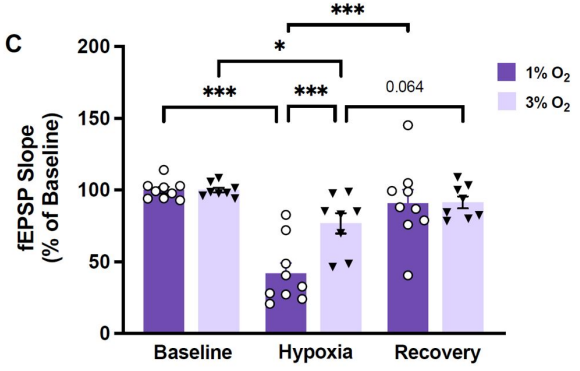

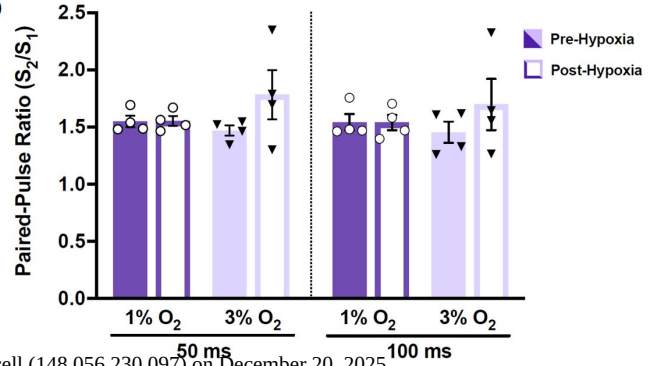

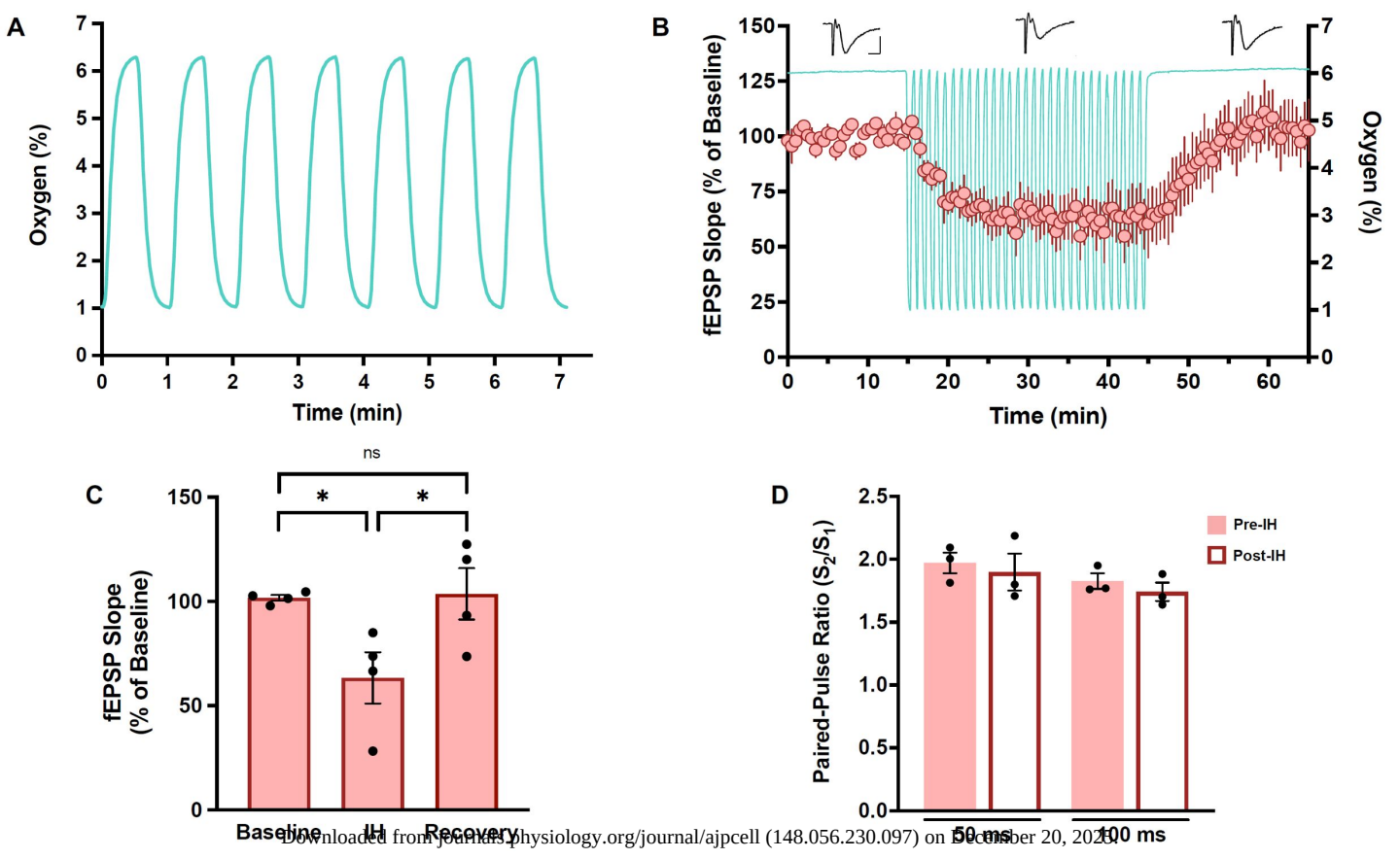

A Novel Platform for Dynamic Oxygen Modulation during *Ex Vivo* Brain Recordings

OxySlice Recording Chamber

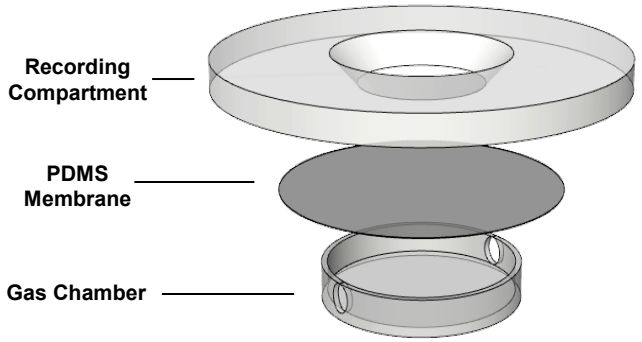

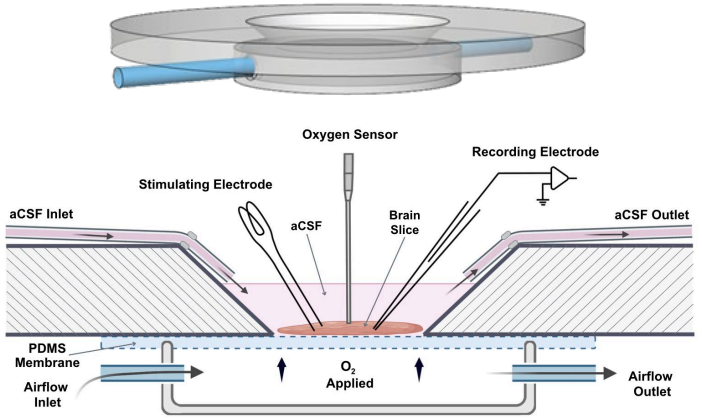

Oxygen-dependent synaptic activity

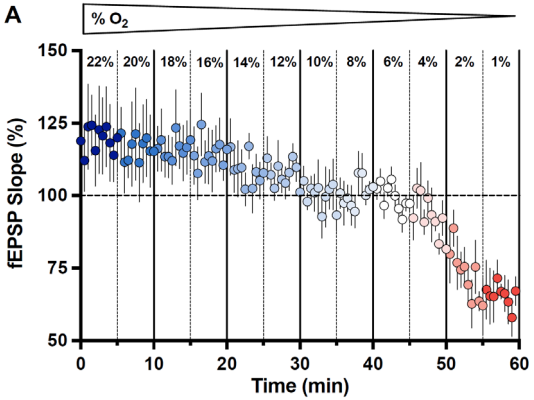

Dynamic oxygen modulation and neuronal response

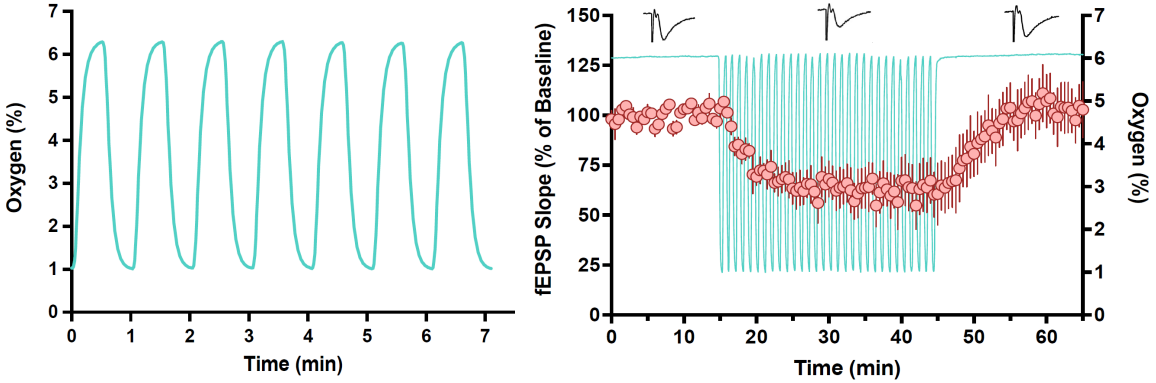

The OxySlice Recording Chamber provides precise, dynamic control of oxygen levels for studying neuronal function